AIP | Journal of Applied Physics

Current perpendicular magnetoresistances of NiFeCo and NiFe "Permalloys"

L. Vila, W. Park, J. A. Caballero, D. Bozec, R. Loloee, W. P. Pratt Jr., and J. Bass

Citation: Journal of Applied Physics **87**, 8610 (2000); doi: 10.1063/1.373586
View online: http://dx.doi.org/10.1063/1.373586
View Table of Contents: http://scitation.aip.org/content/aip/journal/jap/87/12?ver=pdfcov
Published by the AIP Publishing

Current perpendicular magnetoresistances of NiFeCo and NiFe ''Permalloys''

L. Vila, W. Park, J. A. Caballero, D. Bozec, R. Loloee, W. P. Pratt, Jr., and J. Bass[a)]
Department of Physics and Astronomy, Center for Sensor Materials, and Center for Fundamental Materials Research, Michigan State University, East Lansing, Michigan 48824-1116

(Received 7 December 1999; accepted for publication 14 March 2000)

Measurements are presented of the 4.2 K current perpendicular specific resistances (area times resistance) and magnetoresistances of a series of $Ni_{66}Fe_{13}Co_{21}$=Py′-based symmetric exchange-biased spin valves and Py′–Co hybrid spin valves. The behaviors of both kinds of Py′-based spin valves are similar to those for comparable $Ni_{84}Fe_{16}$=Py-based spin valves. The low temperature giant magnetoresistive parameters of Py′ must, thus, be similar to those for Py, suggesting that Py′ should be a viable alternative to Py for technological uses. © *2000 American Institute of Physics.* [S0021-8979(00)04912-4]

I. INTRODUCTION

Because of its low coercive (H_c) and saturation (H_s) magnetic fields, and its good giant magnetoresistive (GMR) characteristics, Permalloy (Py)=$Ni_{100-x}Fe_x$ with $x\sim 20$, is a crucial component of most GMR based technologies.[1] $Ni_{65}Fe_{15}Co_{20}$, which we designate as Py′, is a Py variant with somewhat higher room temperature values of H_c and H_s than Py. If the GMR parameters of Py′ are comparable to those of Py, then Py′ could be a superior alternative for some applications.

From current perpendicular to the plane (CPP) measurements on lithographically prepared samples of $[Co/Cu/Py'/Cu]_{10}$ hybrid spin valves with equal Co and Py′ thicknesses, t_{Cu} and t_{Py}, Krebs *et al.*[2] estimated low temperature GMR parameters for Py′ much smaller than those we derived for Py.[3] However, their analysis required a number of assumptions, namely that: (a) they could properly correct for a nonuniform current distribution in their samples; (b) they achieved the parallel (P) and antiparallel (AP) magnetic states needed to maximize the MR; (c) they could use parameters derived by others[3,4] to describe their sputtered Co and the Co/Cu and Py′/Cu interfaces; (d) the contact resistances to their samples were negligible; and (e) the length for spin-memory loss (spin-diffusion length $l_{sf}^{Py'}$) in Py′ is much longer than their Py′ layer thicknesses.

The large difference between their parameters for Py′ and ours for Py, coupled with the uncertainty engendered by the assumptions listed above, led us to reexamine Py′ $=Ni_{65}Fe_{15}Co_{20}$ using the alternative technique of crossed superconducting Nb strips.[5] Our reexamination has the advantages of: (a) a uniform CPP current density over the sample area A; (b) more reliable achievement of AP and P magnetic states; (c) direct knowledge of the Co and Co/Cu parameters for samples made in our system with our techniques; (d) knowledge of our contact resistances; and (e) the ability to simultaneously estimate $l_{sf}^{Py'}$.

In this article we report CPP-MR measurements of sputtered symmetric exchange-biased spin valves (EBSVs) of Py′ (equal thicknesses of the two Py′ layers), and of hybrid spin valves of Py′ and Co with fixed Co thicknesses (t_{Co} $=2$ or 3 nm) and also with equal thicknesses of Co and Py′. From these data we conclude that the GMR parameters of our Py′ are close to those for Py and much larger than those inferred by Krebs *et al.* To provide a concurrent comparison standard, we also measured the CPP-MRs of newly sputtered symmetric exchange-biased spin valves of Py, for which we found slightly larger MRs than those we previously reported.[3] The fluctuations in the new and old Py data overlap, but the differences in their averages lie just beyond our expected uncertainties. Fortunately, the only revised parameter needed to fit the new Py data lies well within our previously estimated uncertainty.

II. MATERIAL, TECHNIQUES, SAMPLES, AND ACHIEVING THE MAGNETIC STATES OF INTEREST

A nominal $Ni_{65}Fe_{15}Co_{20}$(=Py′) alloy target was obtained from Angstrom Sciences Inc. Electron microprobe analysis of sputtered thin films yielded concentrations of $Ni_{66}Fe_{13}Co_{21}$, close to the desired concentrations. Van der Paaw measurements of the residual resistivities of these thin films at 4.2 K gave $\rho_{Py}=98\pm 10\,n\Omega$ m. A linear fit to values of AR vs $t_{Py'}$ for sandwiches of Py′ between 250-nm-thick Nb layers gave a slope of $\rho_{Py'}=82\pm 5\,n\Omega$ m and intercept $7.5\pm 1\,f\Omega\,m^2$. For our best estimate of $\rho_{Py'}$ we choose the average of the two values: $\rho_{Py'}=90\pm 15\,n\Omega$ m. The observed intercept is consistent with the $7.0\pm 1.5\,f\Omega\,m^2$ measured for Nb/Py.[3] In Py, correction for a finite spin-diffusion length led to a Nb/Py interface specific resistance of $2AR_{Nb/Py}=6.0\,f\Omega\,m^2$ (Ref. 3) smaller than the intercept. For simplicity of CPP-MR analysis, we take this parameter (to which the data are not very sensitive) for Py′ to be the same as for Py, $2AR_{Nb/Py'}=6.0\,f\Omega\,m^2$. The two independently estimated values of $\rho_{Py'}$ are mutually consistent, but smaller than the $\rho_{Py'}=129\,n\Omega$ m listed in Ref. 2. However, since all of the values are probably dominated by sputtering-induced

a)Author to whom correspondence should be addressed; electronic mail: bass@pa.msu.edu

defects, they are within the differences expected for samples prepared in different laboratories. As an example of the differences that can occur over years in even the same laboratory, our new test films of Py gave $\rho_{Py}=100\pm10\,n\Omega\,m$, lower than, but overlapping with, both the $111\pm8\,n\Omega\,m$ previously directly measured by the Van der Paaw technique[6] and the $123\pm40\,n\Omega\,m$ derived from Py/Co hybrid data neglecting any finite l_{sf}^{Py}.[6]

Our CPP-MR sample structure and the techniques used to prepare and measure our multilayer samples have been described in detail elsewhere.[5] We note only that we used our standard ~1-mm-wide crossed superconducting Nb strip technique, which limits our measurements to cryogenic temperatures—for the present studies to 4.2 K, and that the Cu thickness used to separate the Py′ or Py layers was held constant at the large value of $t_{Cu}=20\,nm$ to minimize any exchange coupling between those layers.

As always, measurements of the cross-sectional area A $\sim1.1\,mm^2$ through which the CPP current flows let us determine the specific resistances, *AR*, of interest.[7,8] Since the previous CPP-MR data on Py were published,[3] we have upgraded our argon purification system, changed to a new set of masks because the old ones were deteriorating, and reprogrammed our computer using Labview to better standardize and simplify the programming of samples. These changes probably contributed to the small systematic differences found between our old and new Py data noted above, the latter having been stable now for over a year in studies by several different students.

Important to the analysis we present below is the ability to achieve the two magnetic states of primary interest, where the magnetizations of adjacent layers are single domain and parallel (P) or antiparallel (AP) to each other. The P state occurs naturally for a large enough *H*. We have used two techniques to approach the more difficult AP states. The first technique, symmetric (EBSVs)[3,9]—[FeMn(8)/Py′($t_{Py'}$)/Cu(20)/Py′($t_{Py'}$)]—utilizes an 8-nm-thick layer of the antiferromagnet FeMn to ''pin'' the magnetization of an adjacent pinned Py′ layer to a higher field than is needed to reversibly reorient that of a well separated ''free'' Py′ layer. To ensure the proper crystal structure of FeMn for pinning,[10] the FeMn was grown on a 10 nm Cu layer[11] on top of the bottom Nb strip.

The second technique, hybrid spin valves of the form $[Co(2or3)/Cu(20)/Py'(t_{Py'})/Cu(20)]_N$ (with $N=8$ or 10 quadrilayers) involves a combination of two different ferromagnetic (F) metals, Co and Py′, with the Co thickness kept small enough ($t_{Co}=2$ or 3 nm) so that its H_s is larger than those of the thicker Py′ layers of main interest. The Py′ layers then reverse before the Co ones.

Figure 1(a) shows how *AR* varies with magnetic field *H* for an EBSV as *H* is swept through both a minor loop (where only the free layer reverses) and a major loop (where both layers reverse). At 4.2 K, both we and Krebs *et al.*[2] find that sputtered free Py′ requires a larger reversing field than is typical for sputtered free Py,[12] making the achievement of an AP state not quite as easy as for Py. Nonetheless, the relative flatness of the ''top'' of the curve shows that we achieve at least a close lower bound to the AP state. Figure 1(b) shows

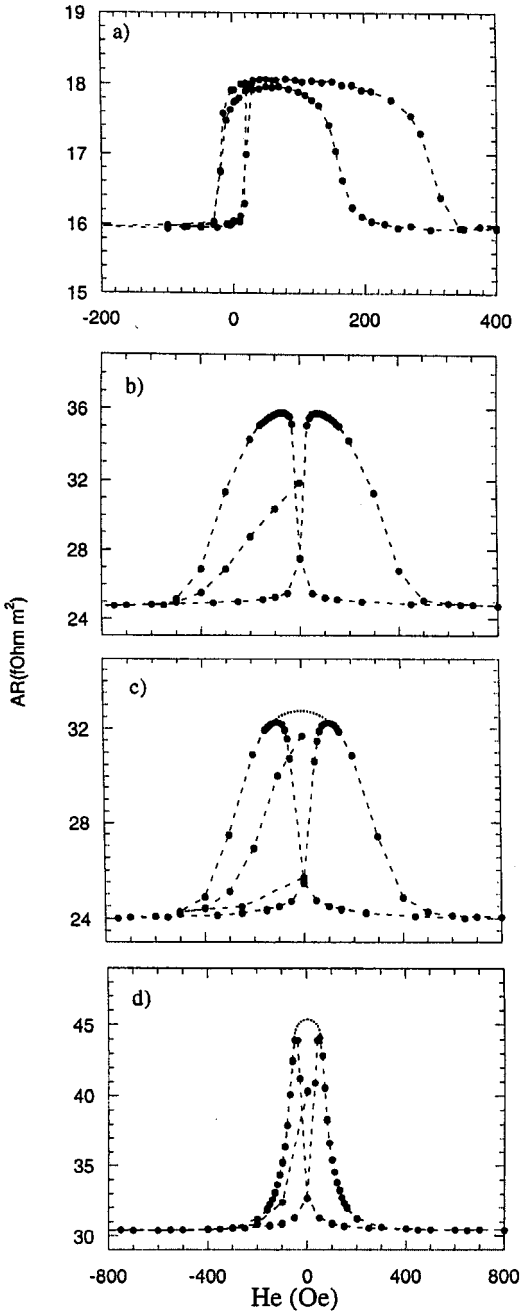

FIG. 1. $AR(H)$ vs H for: (a) a symmetric EBSV with $t_{Py'}=12$ mm; (b) a hybrid SV with $N=8$, $t_{Co}=2$ nm, and $t_{Py'}=8$ nm (c) a hybrid SV with $N=8$, $t_{Co}=2$ nm, and $t_{Py'}=3$ nm, and (d) a hybrid SV with $N=10$ and $t_{Co}=t_{Py'}=6$ nm. In each case, the lowest value of *AR* corresponds to AR(P). In 1(a) and 1(b) the highest value of *AR* is our estimate of AR(AP). In 1(c) and 1(d) the dotted curves indicate extrapolations to our ''best estimates'' of AR(AP).

the variation of *AR* for a hybrid SV with $N=8$, $t_{Co}=2$ nm and moderately thick $t_{Py'}=8$ nm. The asymmetric peak shape, composed of a sharp rise as *H* increases from zero, followed by a much slower fall after the peak, is evidence of a close approach to an AP state. We take these two sets of data as closely approximating the quantities of interest: AR(AP), AR(P), and their difference $A\Delta R=AR(AP)-AR(P)$. In contrast, Fig. 1(c) shows the peaks in *AR* for a hybrid sample with $N=8$, $t_{Py'}=2$ and $t_{Co}=3$ nm and Fig.

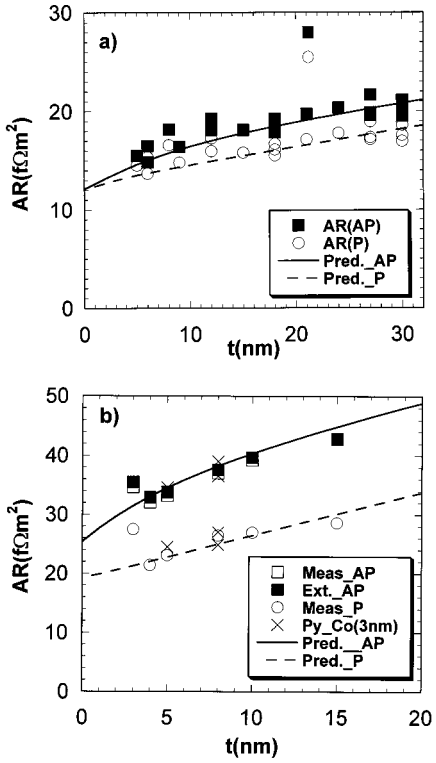

FIG. 2. AR(AP) (squares) and AR(P) (circles) vs t_{Py}. (a) Symmetric Py′ EBSVs. (b) Hybrid Py′-based SVs with $t_{\mathrm{Cu}}=3$ nm—open squares are measured quantities and filled squares are extrapolations to AR(AP) as illustrated in Fig. 1. The crosses are previously published data for nominally identical hybrid spin valves except with Py instead of Py′. The solid and dashed curves are the predicted values of AR(AP) and AR(P) for the Py′ SVs using the parameters specified.

1(d) shows the peaks for a Co and Py′ sample with $N=10$ and $t_{\mathrm{Co}}=t_{\mathrm{Py}'}=6$ nm (made to compare with similar data in Ref. 2). In these cases, the more nearly symmetric peak shapes indicate that these peaks do not represent fully AP states. Here, AR(peak) sets only a lower bound on AR(AP). The dashed curves indicate our attempts to estimate AR(AP) by extrapolation.

III. MAGNETORESISTANCE DATA

Figure 2(a) shows our measured values of AR(P) and AR(AP) vs $t_{\mathrm{Py}'}$ for our symmetric (Py′/Cu/Py′) EBSVs and Fig. 2(b) shows the same quantities for the hybrid SVs with $N=8$ and fixed $t_{\mathrm{Co}}=3$ nm. Figure 3 compares values of $A\Delta R$ vs $t_{\mathrm{Py}'}$ for the Py′-based EBSVs of Fig. 2(a) with those versus t_{Py} for the companion symmetric Py-based EBSVs. Figure 4 shows $A\Delta R$ vs $t_{\mathrm{Py}'}$ for hybrid Py′-based spin valves with $N=8$ and fixed $t_{\mathrm{Co}}=2$ nm (open squares=data as measured; filled squares=data corrected as described in Fig. 1) or 3 nm (open circles=data as measured; filled circles=corrected data), along with data for two Py thicknesses (crosses) from a prior study of otherwise nominally identical [Co/Cu/Py/Cu], hybrid spin valves with $t_{\mathrm{Co}}=3$ nm.[6]

We consider first the Py-based data of Fig. 3. The dashed curve in Fig. 3 shows that the ''best fit'' to our older Py data[3] falls slightly below the new Py data. The dotted curve

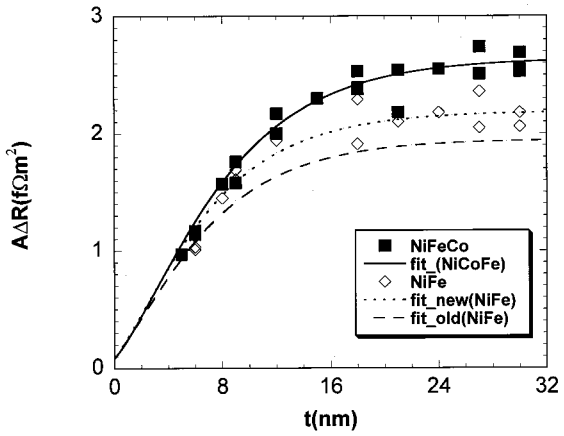

FIG. 3. $A\Delta R$ vs $t_{\mathrm{Py}'}$ or t_{Py} for symmetric EBSVs with Py′ (filled squares) or Py (open diamonds). The dashed curve indicates the best fit to previously published data for symmetric Py-based EBSVs (see Ref. 3). The dotted curve through the Py data indicates a fit to the new data changing only β_{Py} from 0.73 to 0.76. The solid curve through the Py′ data indicates a fit using exactly the same parameters as for Py, except with $\rho_{\mathrm{Py}'}=90$ nΩ m instead of $\rho_{\mathrm{Py}}=123$ nΩ m and with $\beta_{\mathrm{Py}'}=0.82$ instead of $\beta_{\mathrm{Py}}=0.76$.

through the new Py data represents our previous parameters for Py with finite $l_{\mathrm{sf}}^{\mathrm{Py}}=5.5$ nm,[3] except with the bulk anisotropic parameter $\beta_{\mathrm{Py}}=(\rho_{\mathrm{Py}}^{\downarrow}-\rho_{\mathrm{Py}}^{\uparrow})/(\rho_{\mathrm{Py}}^{\downarrow}+\rho_{\mathrm{Py}}^{\uparrow})$ increased from our old best estimate of 0.73 ± 0.07 to the value 0.76 ± 0.07, to conform both with the data shown (which by itself would give a best fit of 0.75) and additional data taken over the past year. The terms $\rho_{\mathrm{Py}}^{\downarrow}$ and $\rho_{\mathrm{Py}}^{\uparrow}$ are the resistivities for electrons with spins antiparallel (↓) or parallel (↑) to the local layer magnetization **M**. This small change in β_{Py} fits the new Py data well. As in previous work, we assume that the full thickness of the Py (or Py′) layer next to the FeMn contributes to the CPP-MR. Reducing this thickness by a few monolayers to an ''effective'' thickness due to interfacial intermixing would lead to a modest modification of parameters that we do not consider here.

We turn now to the variation of the Py′ data with $t_{\mathrm{Py}'}$. Figures 2(a) and 2(b) show that AR(P) increases closely lin-

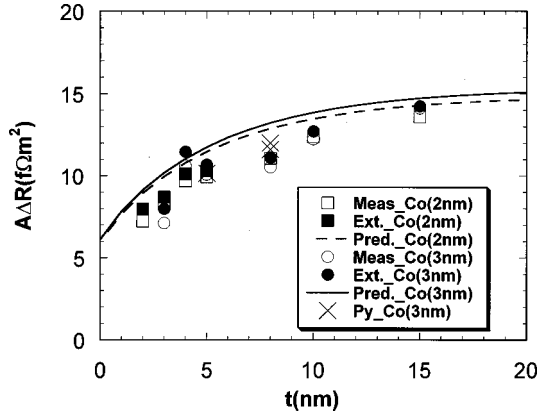

FIG. 4. $A\Delta R$ vs $t_{\mathrm{Py}'}$ for Py′-based hybrid SVs with $t_{\mathrm{Co}}=2$ nm (squares) or 3 nm (circles). Open symbols are measured quantities and filled symbols are extrapolations to AR(AP) as illustrated in Fig. 1. The crosses are data for equivalent Py-based hybrid SVs with $t_{\mathrm{Co}}=3$ nm. The dashed and solid curves are the predictions for $t_{\mathrm{Co}}=2$ nm and 3 nm using the Py′ parameters given.

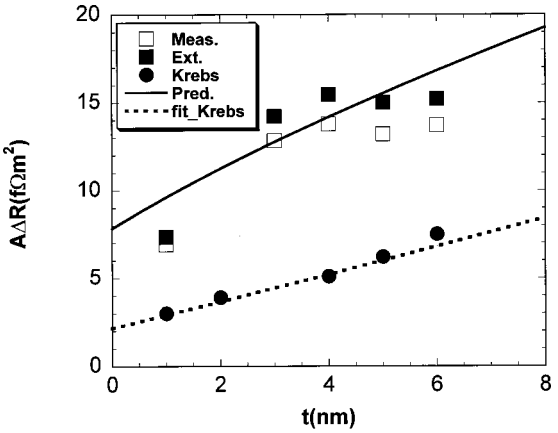

FIG. 5. $A\Delta R$ vs $t_{\mathrm{Py}'}$ for hybrid SVs with $t_{\mathrm{Co}}=t_{\mathrm{Py}'}$. Open squares are our measured quantities and filled squares are extrapolations to $AR(\mathrm{AP})$ as illustrated in Fig. 1. The solid curve is the prediction for these data using the parameters described in the text. The filled circles are the data for nominally equivalent samples from Krebs *et al.* (see Ref. 2). The dashed line is a fit to the Krebs data using our parameters but with an assumed total lead specific resistance of 33 $\mathrm{f\Omega\,m^2}$.

early with $t_{\mathrm{Py}'}$ as expected, and that $AR(\mathrm{AP})$ increases more slowly than linearly. Figures 3 and 4 show that the forms of the variation of $A\Delta R$ with $t_{\mathrm{Py}'}$ for Py′ are very similar to those of $A\Delta R$ with t_{Py} for Py. In Fig. 3, the Py′ data are slightly larger than the Py data. In Fig. 4, the comparable Py and Py′ data are very similar.

IV. ANALYSIS AND DERIVATION OF PARAMETERS

Because of the similarity in behaviors of the Py′ and Py data of Figs. 2–4, we chose to analyze the Py′ data assuming that all but two of the parameters for Py′ are the same as those given for Py in Ref. 3, including the spin-diffusion length $l_{\mathrm{sf}}^{\mathrm{Py}}=l_{\mathrm{sf}}^{\mathrm{Py}'}=5.5\,\mathrm{nm}$. From the measured Py′ resistivity we fixed $\rho_{\mathrm{Py}'}=90\,\mathrm{n\Omega\,m}$. We also fixed the parameters for Co at the best fit values given in Ref. 6. These assumptions left only a single adjustable parameter, the ''bulk anisotropy parameter'' $\beta_{\mathrm{Py}'}=(\rho_{\mathrm{Py}'}^{\downarrow}-\rho_{\mathrm{Py}'}^{\uparrow}/(\rho_{\mathrm{Py}'}^{\downarrow}+\rho_{\mathrm{Py}'}^{\uparrow})$.[5,8] We determined this parameter by fitting the Py′ data of Fig. 3 numerically with the appropriately derived equations based on the analysis of Valet and Fert.[8] The solid curve in Fig. 3 corresponds to a ''best value'' of $\beta_{\mathrm{Py}'}=0.82$.

This procedure has fixed all of the parameters for both Py′ and Co. We can then ask what ''predictions'' we make for the curves for $AR(\mathrm{AP})$, $AR(\mathrm{P})$, and $A\Delta R$ in Figs. 2 and 4. The results for the appropriate Valet and Fert analyses are shown in Fig. 2 as solid curves for $AR(\mathrm{AP})$ and dashed curves for $AR(\mathrm{P})$ and in Fig. 4 as solid or dashed curves for $A\Delta R$. Since these curves were all predicted with no adjustability whatsoever, and the estimated values of $AR(\mathrm{AP})$ and $A\Delta R$ in Figs. 2 and 4 are subject to the uncertainties described above, the agreements between the data and the curves are encouragingly good. Given the combination of: (a) the agreements between the data and predictions in Figs. 2 and 4; (b) the uncertainty in some of the values of $AR(\mathrm{AP})$ in Figs. 2(b) and 4 as described above; and (c) the range of fits that we could obtain by varying the parameters for Co within their uncertainties, we decided that there was no advantage to trying more formal least-square fits to the data. We simply conclude that the parameters for $Ni_{66}Fe_{13}Co_{21}$ are similar to those we previously published for Py, except that our best estimate of $\rho_{\mathrm{Py}'}=90\pm10\,\mathrm{nm}$ is a little smaller than ρ_{Py} and our best estimate of $\beta_{\mathrm{Py}'}=0.82$ is a little larger than our slightly revised value of $\beta_{\mathrm{Py}}=0.76\pm0.07$.

As a further cross check on our parameters, Fig. 5 compares our measured (open squares) and extrapolated (filled squares) estimates of $A\Delta R$ vs $t=t_{\mathrm{Co}}=t_{\mathrm{Py}'}$ for symmetric hybrid spin valves with $N=10$ with our predictions (solid curve) using the same parameters just described. Given the uncertainties in the extrapolations, and the visible fluctuations in the data, the agreement is quite satisfactory. Shown also in Fig. 5 are the data of Krebs *et al.*[2] for nominally equivalent samples. Both our directly measured and extrapolated values are much larger than theirs. We do not know why the data of Krebs *et al.* are so much smaller than ours. As an example of one possible explanation, the dashed line indicates the values of $A\Delta R$ that would be obtained using our parameters, but replacing our lead specific resistance of $2AR_{\mathrm{Nb/Co}}=6\,\mathrm{f\Omega\,m^2}$ (Ref. 3) with a lead specific resistance of 33 $\mathrm{f\Omega\,m^2}$.

V. SUMMARY AND CONCLUSIONS

We have measured the specific resistances $AR(\mathrm{AP})$, $AR(\mathrm{P})$, and $A\Delta R$ for a series of $Ni_{66}Fe_{13}Co_{21}$=Py′-based symmetric EBSVs and Py′–Co hybrid spin valves. All three quantities are similar to those that we find for $Ni_{80}Fe_{20}$=Py-based symmetric spin valves and Py–Co hybrid spin valves. We conclude that the low temperature GMR parameters of Py′ are similar to those of Py≈$Ni_{80}Fe_{20}$. More detailed analysis gives $\rho_{\mathrm{Py}'}=90\,\mathrm{n\Omega\,m}$, slightly smaller than the equivalent value for Py, and $\beta_{\mathrm{Py}'}\approx0.82$, slightly larger than a revised best estimate of $\beta_{\mathrm{Py}}\approx0.76$. Since there is no *a priori* reason to expect the GMR performance of Py′ to decrease more rapidly with temperature than that of Py, Py′ looks likely to be a viable alternative to Py for technological uses.

ACKNOWLEDGMENTS

This research was supported by the U.S. NSF under MRSEC Grant Nos. 94-00417 and 98-09688, and DMR Grant Nos. 94-23795 and 98-20135, and by the MSU CSM and MSU CFMR.

[1] See, e.g., J. M. Daughton, J. Magn. Magn. Mater. **192**, 334 (1999).
[2] J. J. Krebs, W. Vavra, G. A. Prinz, S. F. Cheng, and A. Fink, J. Appl. Phys. **79**, 6084 (1996).
[3] W. P. Pratt, Jr., S. D. Steenwyk, S. Y. Hsu, W.-C. Chiang, A. C. Schaefer, R. Loloee, and J. Bass, IEEE Trans. Magn. **33**, 3505 (1997); S. D. Steenwyk, S. Y. Hsu, R. Loloee, J. Bass, and W. P. Pratt, Jr., J. Magn. Magn. Mater. **170**, L1 (1997).
[4] W. P. Pratt, Jr., S.-F. Lee, P. Holody, Q. Yang, R. Loloee, J. Bass, and P. A. Schroeder, J. Magn. Magn. Mater. **126**, 406 (1993).
[5] S. F. Lee, Q. Yang, P. Holody, R. Loloee, J. H. Hetherington, S. Mahmood, B. Ikegami, K. Vigen, L. L. Henry, P. A. Schroeder, W. P. Pratt, Jr., and J. Bass, Phys. Rev. B **52**, 15426 (1995).

[6] W. P. Pratt, Jr., Q. Yang, L. L. Henry, P. Holody, W.-C. Chiang, P. A. Schroeder, and J. Bass, J. Appl. Phys. **79**, 5811 (1996); Q. Yang, P. Holody, R. Loloee, L. L. Henry, W. P. Pratt, Jr., P. A. Schroeder, and J. Bass, Phys. Rev. B **51**, 3226 (1995).
[7] S. F. Lee, W. P. Pratt, Jr., Q. Yang, P. Holody, R. Loloee, P. A. Schroeder, and J. Bass, J. Magn. Magn. Mater. **118**, L1 (1993).
[8] T. Valet and A. Fert, Phys. Rev. B **48**, 7099 (1993).
[9] B. Dieny, V. S. Speriosu, S. Metin, S. S. P. Parkin, B. A. Gurney, P. Baumgart, and D. R. Wilhoit, J. Appl. Phys. **69**, 4774 (1991).
[10] The first sputtered sample in each EBSV sputtering run usually gave an unusually large AR(AP) and AR(P), along with wider fluctuations of $A\Delta R$ than usual. Because we fear that these larger *AR*s mean that the FeMn did not fully adopt the proper crystal structure for pinning, Figs. 2(a) and 3 do not contain any data from first sputtered EBSV samples. We note, however, that including those data would not significantly change any of the analysis or conclusions in this article.
[11] C. Tang and K. Lee, J. Appl. Phys. **53**, 2605 (1982).
[12] S. D. Steenwyk, S. Y. Hsu, R. Loloee, J. Bass, and W. P. Pratt, Jr., J. Appl. Phys. **81**, 4011 (1997).